tion and stereochemistry in the chemistry of cyclization, and the enzyme elegantly protects and stabilizes reactive carbocation intermediates. These features are likely to be common to all terpenoid cyclases. Alteration of active site residues in a terpenoid cyclase can result in the formation of aberrant cyclization products, so that the architecture and chemical nature of the substrate binding pocket are critical for channeling the correct cyclization chemistry (*18*). Now that the three-dimensional structure of a terpenoid synthase is available at atomic resolution, we are in a position to test the specific catalytic function of individual amino acids, as well as entire helical subdomains, in structure-based redesign experiments.

REFERENCES AND NOTES

1. L. Ruzicka, *Pure Appl. Chem.* **6**, 493 (1963).
2. D. E. Cane, *Acc. Chem. Res.* **18**, 220 (1985); R. Croteau and D. E. Cane, *Methods Enzymol.* **110**, 383 (1985); D. E. Cane, *Chem. Rev.* **90**, 1089 (1990).
3. Hippocrates, ΠΕΡΙ ΝΟΥΣΩΝ Β (P. Potter, translator) (Harvard Univ. Press, Cambridge, 1988); Pliny, *Naturalis Historiae* (W. H. S. Jones, translator) (Harvard Univ. Press, Cambridge, 1969); C. A. Michie and E. Cooper, *J. R. Soc. Med.* **84**, 602 (1991); P. Dolara *et al.*, *Nature* **379**, 29 (1996).
4. I. Abe, M. Rohmer, G. D. Prestwich, *Chem. Rev.* **93**, 2189 (1993); E. J. Corey *et al.*, *J. Am. Chem. Soc.* **117**, 11819 (1995); E. J. Corey and H. B. Wood, *ibid.* **118**, 11982 (1996); E. J. Corey *et al.*, *ibid.* **119**, 1277 (1997); E. J. Corey *et al.*, *ibid.*, p. 1289.
5. The committed step of paclitaxel (Taxol™) biosynthesis is the generation of taxadiene from geranylgeranyl diphosphate in a reaction catalyzed by taxadiene synthase; X. Y. Lin, M. Hezari, A. E. Knoepp, H. G. Floss, R. Croteau, *Biochemistry* **35**, 2968 (1996).
6. R. Croteau, *Chem. Rev.* **87**, 929 (1987).
7. D. E. Cane *et al.*, *Biochemistry* **33**, 5846 (1994); C. A. Lesburg, M. D. Lloyd, D. E. Cane, D. W. Christianson, *Protein Sci.* **4**, 2436 (1995).
8. L. C. Tarshis, M. Yan, C. D. Poulter, J. C. Sacchettini, *Biochemistry* **33**, 10871 (1994); L. C. Tarshis, P. J. Proteau, B. A. Kellogg, J. C. Sacchettini, C. D. Poulter, *Proc. Natl. Acad. Sci. U.S.A.* **93**, 15018 (1996).
9. D. Reardon and G. K. Farber, *FASEB J.* **9**, 497 (1995).
10. C. M. Starks, K. Back, J. Chappell, J. P. Noel, *Science* **277**, 1815 (1997).
11. C. A. Lesburg, G. Zhai, D. E. Cane, D. W. Christianson, unpublished data.
12. M. N. Ashby and P. A. Edwards, *J. Biol. Chem.* **265**, 13157 (1990).
13. Aqueous Mg^{2+} is known to catalyze the solvolysis of allylic diphosphates even at pH 7.0; L. Chayet, M. C. Rojas, O. Cori, C. A. Bunton, D. C. McKenzie, *Bioorg. Chem.* **12**, 329 (1984).
14. D. E. Cane, C. Abell, A. M. Tillman, *ibid.*, p. 312; D. E. Cane *et al.*, *J. Am. Chem. Soc.* **112**, 4513 (1990); D. E. Cane *et al.*, *Philos. Trans. R. Soc. B.* **332**, 123 (1991); D. E. Cane and S. W. Weiner, *Can. J. Chem.* **72**, 118 (1994).
15. S. S. Dehal and R. Croteau, *Arch. Biochem. Biophys.* **261**, 346 (1988); J. I. M. Rajaonarivony, J. Gershenzon, J. Miyazaki, R. Croteau, *ibid.* **299**, 77 (1992).
16. Models of enzyme-substrate, -intermediate, and -product complexes were prepared by calculating minimum energy conformations along the reaction coordinate of cyclization with MacroModel [F. Mohamadi *et al.*, *J. Comput. Chem.* **11**, 440 (1990)]. Subsequently, these conformers were docked into the pentalenene synthase active site as guided by the strict stereochemical requirements for each step of the cyclization reaction. Buried surface areas were calculated with the use of GRASP [A. Nicholls, K. A. Sharp, B. Honig, *Prot. Struct. Funct. Gen.* **11**, 281 (1991)].
17. S. K. Burley and G. A. Petsko, *Adv. Prot. Chem.* **39**, 125 (1988); D. A. Dougherty, *Science* **271**, 163 (1996).
18. D. E. Cane and Q. Xue, *J. Am. Chem. Soc.* **118**, 1563 (1996); K. Back and J. Chappell, *Proc. Natl. Acad. Sci. U.S.A.* **93**, 6841 (1996).
19. J. Nyborg and A. J. Wonacott, in *The Rotation Method in Crystallography*, U. W. Arndt and A. J. Wonacott, Eds. (North-Holland, Amsterdam, 1977), p. 139.
20. Collaborative Computational Project, Number 4, *Acta Crystallogr.* **D50**, 760 (1994).
21. Z. Otwinowski and W. Minor, *Methods Enzymol.* **276**, 307 (1997).
22. J. P. Abrahams and A. G. W. Leslie, *Acta Crystallogr.* **D52**, 30 (1996).
23. A. T. Brünger, J. Kuriyan, M. Karplus, *Science* **235**, 458 (1987).
24. T. A. Jones, J.-Y. Zou, S. W. Cowan, M. Kjeldgaard, *Acta Crystallogr.* **A47**, 110 (1991).
25. Figures 1 and 2 were prepared with (i) MOLSCRIPT: P. Kraulis, *J. Appl. Crystallogr.* **24**, 946 (1991); and (ii) Raster3D: D. J. Bacon and W. F. Anderson, *J. Mol. Graph.* **6**, 219 (1988); E. A. Merritt and M. E. P. Murphy, *Acta Crystallogr.* **D50**, 869 (1994).

26. We thank G. Farber, A. Jain, Z. Kanyo, W. N. Lipscomb, M. D. Lloyd, P. Lu, P. Sprengler, T. Stams, and G. M. Whitesides for helpful discussions during the course of this investigation and J. Noel for sharing data on the structure of *epi*-aristolochene synthase prior to publication. Supported by grants from the National Institutes of Health. This work is based upon research conducted at the Cornell High Energy Synchrotron Source (CHESS), which is supported by the National Science Foundation under award DMR-9311772, with the use of the Macromolecular Diffraction at CHESS (MacCHESS) facility, which is supported by award RR-01646 from the National Institutes of Health. Atomic coordinates have been deposited in the Brookhaven Protein Data Bank with accession code 1PS1.

21 March 1997; accepted 1 August 1997

Toroidal Structure of λ-Exonuclease

Rhett Kovall and Brian W. Matthews

Structure determination at 2.4 angstrom resolution shows that λ-exonuclease consists of three subunits that form a toroid. The central channel is funnel shaped, tapering from an inner diameter of about 30 angstroms at the wider end to 15 angstroms at the narrow end. This is adequate to accommodate the DNA substrate and thus provides a structural basis for the ability of the enzyme to sequentially hydrolyze thousands of nucleotides in a highly processive manner. The results also suggest the locations of the active sites and the constraints that limit cleavage to a single strand.

DNA exonucleases participate in DNA replication, repair, and recombination (*1*). In particular, processive 5′ to 3′ single-stranded DNA exonucleases are essential for generating early DNA intermediates in many pathways of prokaryotic and eukaryotic homologous recombination (*2*). Bacteriophage λ encodes its own exonuclease, λ-exonuclease, which facilitates phage DNA recombination through the double-strand break repair (DSBR) and single-strand annealing pathways (*3*, *4*).

λ-Exonuclease binds a free end of double-stranded DNA and degrades one of those strands in the 5′ to 3′ direction, releasing 5′ mononucleotides at a rate of ~12 nucleotides per second (*5*). The protein requires Mg^{2+} and the 5′-terminal phosphate for activity (*5*). λ-Exonuclease is highly processive; it remains bound to DNA while it sequentially cleaves ~3000 nucleotides (*6*).

In the DSBR pathway of recombination, the long 3′ single-stranded overhangs created by λ-exonuclease are bound by the *Escherichia coli* recombination protein RecA. These single-stranded DNA RecA filaments then undergo strand exchange with a homologous piece of double-stranded DNA (*3*, *7*). In the case of single-strand annealing recombination, the creation of 3′ overhangs exposes two homologous single-stranded regions of DNA that anneal to form the recombinant double-stranded molecule independently of RecA (*4*, *7*). Analogous pathways of recombination in yeast (*8*), *Xenopus* oocytes (*9*), and mammalian cells (*10*) also require a processive 5′ to 3′ single-stranded DNA exonuclease.

Here we describe the crystal structure of λ-exonuclease determined at 2.4 Å resolution with the use of multiple isomorphous replacement and anomalous dispersion (Table 1). The asymmetric unit of the crystal structure shows that λ-exonuclease, known to be a multimer (*11*), is indeed a trimer with noncrystallographic threefold symmetry (Fig. 1A). The three protein subunits form a toroid, with a tapered channel passing through the middle. At the wide end of the channel, the diameter is about 30 Å, and it decreases to about 15 Å at the narrow end. Although the crystal structure determined does not include DNA, it appears that the tapered channel is large enough to accommodate double-stranded DNA at the wide end but

Institute of Molecular Biology, Howard Hughes Medical Institute, and Department of Physics, University of Oregon, Eugene, OR 97403, USA.

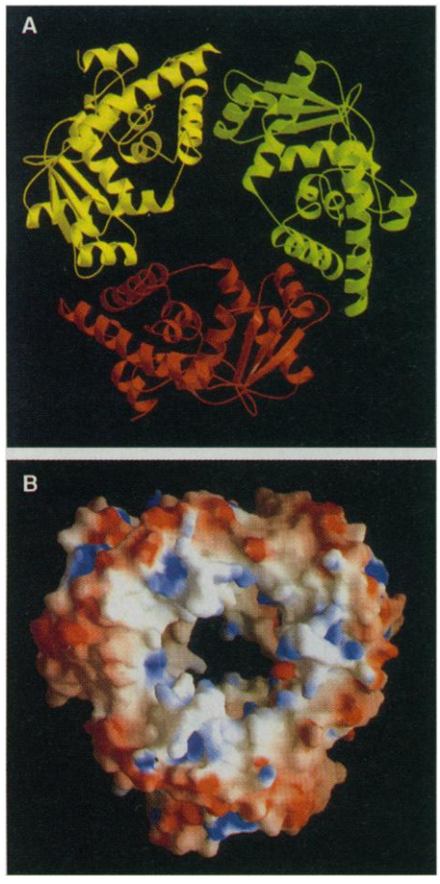

Fig. 1. (**A**) Ribbon diagram of the trimeric λ-exonuclease structure as contained within the asymmetric unit of the crystal. The threefold axis is approximately perpendicular to the plane of the page. The figure was created with MOLSCRIPT (*31*) and rendered with RASTER3D (*32*). (**B**) Electrostatic potential surface of λ-exonuclease determined by using GRASP (*33*) and viewed toward the wider opening of the central channel. The most positive region is dark blue and the most negative region is deep red.

can accommodate only single-stranded DNA at the other end (Fig. 2). The correspondence between the dimensions of DNA and the protein channel suggests that the enzyme actually encloses its substrate.

Despite being a DNA-binding protein, the molecule carries an overall negative charge. This negative potential, however, is concentrated away from the channel (Fig. 1B).

The structure suggests an explanation for the processivity of λ-exonuclease (Fig. 2). Once cleavage is under way the protein remains strung like a bead on the nondigested strand of DNA and remains bound until an end of the DNA is reached or until the protein dissociates into monomers. Conversely, the trimer can bind a new DNA strand only at a double-stranded break, which explains the resistance of closed circular DNA substrates to hydrol-

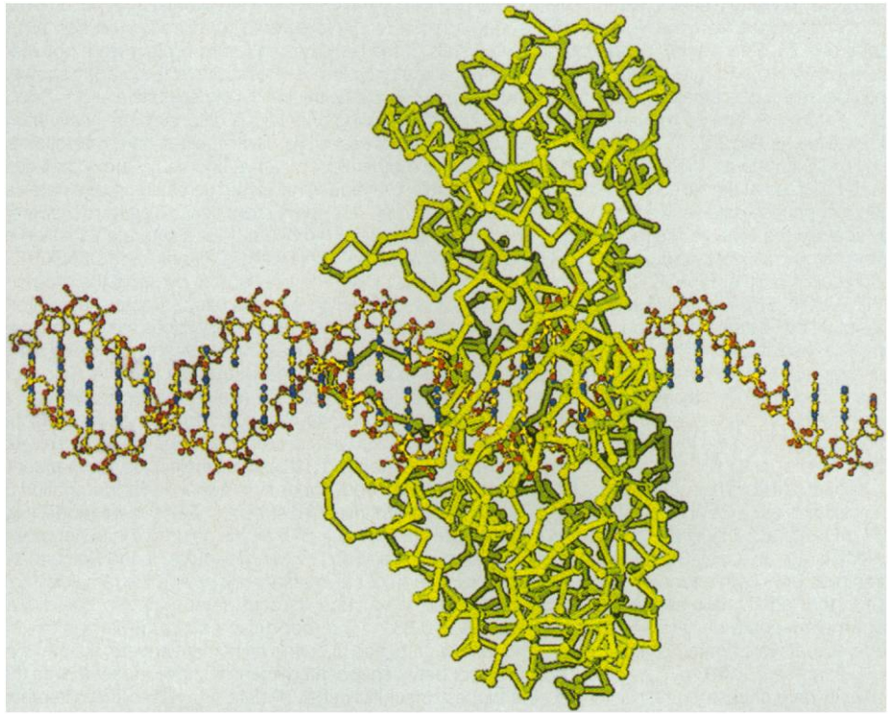

Fig. 2. Proposed model for interaction of λ-exonuclease with DNA, created with the program O (*28*). The long axis of the DNA coincides or approximately coincides with the threefold axis of the protein trimer. The tapered channel within the toroidal structure of the protein is wide enough to accommodate double-stranded DNA at one end but only single-stranded DNA at the other.

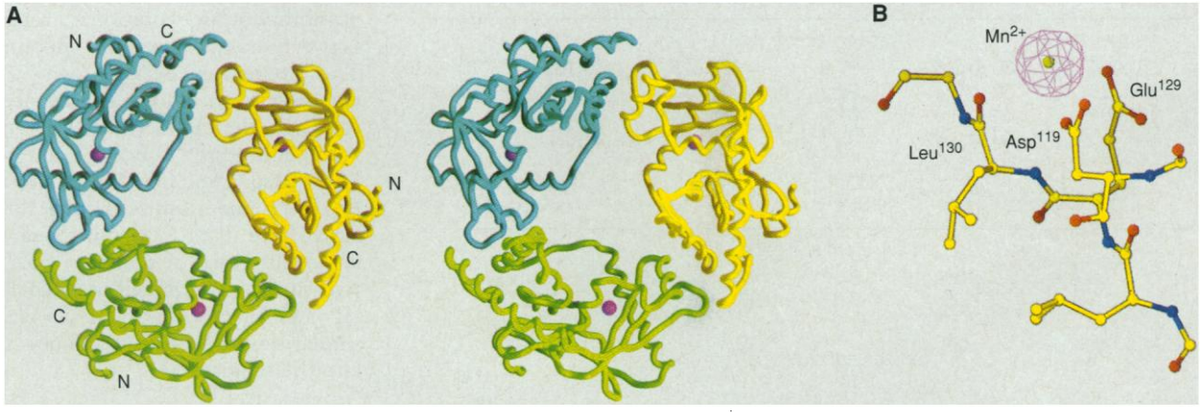

Fig. 3. (**A**) Stereo drawing showing the overall fold of the trimer of λ-exonuclease with manganese ions (magenta spheres) bound at the putative active sites. The figure was created with GRASP (*33*). (**B**) Map showing location of bound manganese. Structure amplitudes ($F_{O,Mn}$) were measured for crystals of λ-exonuclease soaked for 7 days in the mother liquor (Table 1) containing 10 mM $MnCl_2$. Electron density (magenta) was calculated with coefficients ($F_{O,Mn} - F_{O,Nat}$) and phases from the refined native structure. The resolution was 2.4 Å and the map was contoured without averaging at 10σ where σ is the root-mean-square density throughout the unit cell. The Mn^{2+} (green sphere) is bound by the side chains of Asp^{119} and Glu^{129} and the backbone carbonyl of Leu^{130}. Produced with the program O (*28*).

ysis (6). As early as 1968, in discussing possible mechanisms for the processive degradation of nucleic acid chains, Klee and Singer (12) stated that "physical entrapment of the substrate within the enzyme structure [is a] possible mechanism [for processivity]." Two DNA replication processivity factors, proliferating cell nuclear antigen from *Saccharomyces cerevisiae* and the β subunit of *E. coli* polymerase III, also have toroidal structures (13). These proteins are thought to enclose the DNA and to function as sliding clamps, enhancing the processivity of DNA polymerase.

Table 1. X-ray data collection, heavy atom, and structure refinement statistics. A construct of λ-exonuclease containing a 20–amino acid NH_2-terminal histidine tag was kindly provided by Novagen, and the protein was overexpressed in the *E. coli* cell line BL21(DE3)pLysS (Novagen). The protein was purified by passing a cellular extract over a nickel affinity column (His·bind resin, Novagen) in accordance with the protocols from the Novagen pET system manual (ed. 4) followed by gel filtration (HiLoad 16/60 Superdex 75, Pharmacia). Diffraction quality crystals of the histidine-tag fusion protein were obtained from 1.2 M $(NH_4)_2SO_4$, 0.2 M NaCl, 0.1 M sodium acetate at pH 4.7. Precession photography showed the space group to be either $P4_12_12$ or its enantiomer $P4_32_12$, with unit cell dimensions $a = b = 156.7$ Å, $c = 131.7$ Å. The correct space group, determined by using anomalous data from the heavy atom derivatives, is $P4_12_12$. The crystals proved to be radiation-sensitive and required data collection at −170°C with the addition of 25% (v/v) glycerol to the mother liquor. Native and heavy atom data sets were collected at the NSLS beamline X4A at Brookhaven. An additional higher resolution native data set and manganese data set were collected at CHESS beamline A1. Heavy atom derivatives were prepared by soaking the crystals in a mother liquor that contained either 10 mM $GdCl_2$ or a saturated solution of ethylmercury thiosalicylic acid (EMTS). Native and derivative data sets were integrated with DENZO (22) and scaled in SCALEPACK (22). Intensities were converted to structure factors by using the program TRUNCATE (23). The CCP4 suite of programs (24) and XTALVIEW (25) were used to locate heavy atom positions by Patterson methods. The heavy atom sites were refined and initial phases were calculated to 3.0 Å resolution with the program MLPHARE (26). The initial map was then solvent flattened by using the program DM (27). At this stage there were clear regions of secondary structure (Fig. 4A). The map was further improved by averaging over the three noncrystallographically related monomers within the asymmetric unit. An entire protein chain (residues 1 to 226) could then be built into the map by using the program O (28). In the initial refinement (29) the three subunits were constrained to be identical. This led to an *R* factor of 28.9% to 2.4 Å resolution, with 3 phosphates and 318 solvent molecules. Subsequently, departures from noncrystallographic symmetry were allowed. There is no evidence for the location of the histidine tag except for two amino acids at the NH_2-termini of two subunits. The current model (Fig. 4B) consists of 5933 total atoms: 5486 protein atoms (226 × 3 = 678 amino acids in the trimer plus 4 histidine tag residues), 3 phosphate ions, 4 acetate ions, and 421 water molecules. In the Ramachandran plot, 94% of the nonglycine amino acids are in the "most favorable" regions and the remaining 6% are in the "additionally allowed" regions (30). For the three subunits considered pairwise, the overall root-mean-square deviation for all protein atoms is 0.88 Å. The root-mean-square deviations for the regions that were restrained between the monomers (*a*, *b*, and *c*) during refinement are *a*:*b*, 0.65 Å; *a*:*c*, 0.57 Å; and *b*:*c*, 0.59 Å. R_{sym} gives the agreement between repeated intensity measurements with the value in parentheses corresponding to the highest resolution shell of data. R_{iso} gives the difference between the structure amplitudes of the derivative and the native protein. FOM is the figure of merit for the individual derivatives (the value for the two derivatives in combination, to 3.0 Å, is 0.53). $R_{c,isom}$ is the lack of closure of the phase triangles divided by the isomorphous differences and $R_{c,anom}$ is the corresponding residual for the anomalous scattering data.

Crystal	Wavelength (Å)	Resolution (Å)	Completeness (%)	No. of observations	Unique reflections	R_{sym} (%)
			Data collection			
Native I	0.984	30 to 2.6	97.9	204,326	48,162	6.4 (28.7)
Native II	0.908	30 to 2.4	98.2	291,671	62,882	5.5 (24.7)
EMTS	0.984	30 to 2.6	64.7	168,955	31,948	7.5 (16.1)
$GdCl_2$	1.710	30 to 3.3	93.1	153,923	23,022	10.1 (25.7)

Derivative	Resolution	R_{iso}	No. of sites	FOM	$R_{c,isom}$	Phasing power	$R_{c,anom}$
			Heavy atom statistics				
EMTS	3.0 Å	26.8%	6	0.42	0.70	1.31	0.66
$GdCl_2$	3.3 Å	27.9%	3	0.47	0.81	0.92	0.62

Refinement statistics	
Resolution	30.0 to 2.4 Å
No. of reflections	62,855
Completeness of data	97.0%
Average discrepancy of bond lengths from ideal values	0.017 Å
Average discrepancy of bond angles from ideal values	2.6°
Average discrepancy of trigonal planes from ideal values	0.019 Å
Average discrepancy of general planes from ideal values	0.018 Å
Crystallographic residual (*R*)	19.8%

The proposed structure of the λ-exonuclease–DNA complex also explains why the degradation is confined to one of the two DNA strands. The threefold symmetry of the trimer aligns all three subunits parallel to the long axis of the DNA. The three active sites therefore are similarly aligned with respect to one strand of DNA but face the other strand of DNA in the opposite orientation.

Although the amino acid residues that are involved in catalysis have yet to be identified biochemically, a manganese ion bound to each protein subunit suggests the location of the magnesium binding site essential for activity and points to the putative locations of the active sites (Fig. 3A). Mn^{2+} can be substituted for Mg^{2+} in λ-exonuclease, albeit with a fourfold reduction in activity (14). The difference in electron density between a crystal of λ-exonuclease soaked in $MnCl_2$ and the native structure (Fig. 3B) indicates that Mn^{2+} is chelated by the side chains of Asp^{119} and Glu^{129} and the backbone carbonyl of Leu^{130}. Further evidence for this metal binding site comes from the gadolinium derivative ($GdCl_2$) (Table 1) for which the binding sites in the trimer are identical to the Mn^{2+} sites. Lanthanides can substitute at magnesium binding sites (14).

The monomer of λ-exonuclease has an α/β fold. A search of the Brookhaven Data Base with the program Dali (15) did not reveal any other protein with the same overall fold. There is included within residues 75 to 205, however, a subdomain of λ-exonuclease that consists of two α-helices and five strands that is similar to the type II restriction endonucleases Eco RV (16) and Pvu II (17). The region of structural homology encompasses the active sites of all three enzymes. This raises the possibility of an evolutionary relationship between exonucleases and endonucleases. The interactions between Mn^{2+}, Asp^{119}, and Glu^{129} in λ-exonuclease are rather similar to the interactions between Mg^{2+}, Asp^{74}, and Asp^{90} in Eco RV and between Mg^{2+}, Asp^{58}, and Glu^{68} in Pvu II. Lys^{92} in Eco RV is important to the function of the active site (18); λ-exonuclease has an analogous lysine at position 131. The active sites of λ-exonuclease, Eco RI, Bam HI, and Klenow fragment (19–21) share similarities in the acidic residues that chelate the required Mg^{2+}.

REFERENCES AND NOTES

1. S. M. Linn, R. S. Lloyd, R. J. Roberts, *Nucleases* (Cold Spring Harbor Laboratory Press, Cold Spring Harbor, NY, ed. 2, 1993).
2. J. E. Haber, *BioEssays* **17**, 609 (1995).
3. F. W. Stahl, I. Kobayashi, M. M. Stahl, *J. Mol. Biol.*

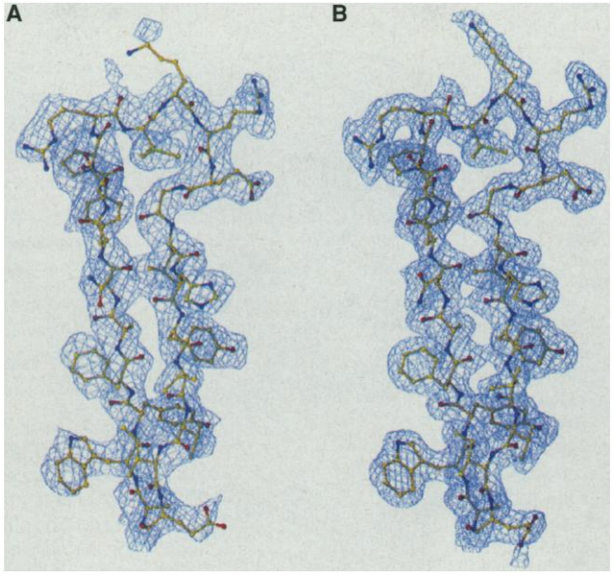

Fig. 4. (**A**) Multiple isomorphous replacement map, including anomalous dispersion, calculated to 3.0 Å resolution and contoured at 1σ showing residues 169 to 190, which form two antiparallel strands connected by a turn. (**B**) Map with coefficients $2F_{O,Nat} - F_c$ calculated to 2.4 Å resolution and contoured at 1σ showing the same region of secondary structure as in (A). The structure amplitudes, F_c, and the phases for the map were calculated from the current refined model (Table 1). Created with the program O (*28*).

181, 199 (1985); F. W. Stahl and M. M. Stahl, *J. Genet.* **64**, 31 (1985); D. S. Thaler, M. M. Stahl, F. W. Stahl, *J. Mol. Biol.* **195**, 75 (1987); N. Takahashi and I. Kobayashi, *Proc. Natl. Acad. Sci. U.S.A.* **87**, 2790 (1990).
4. E. Cassuto and C. M. Radding, *Nature New Biol.* **229**, 13 (1971); E. Cassuto, T. Lash, K. C. Sriprakash, C. M. Radding, *Proc. Natl. Acad. Sci. U.S.A.* **68**, 1639 (1971).
5. C. M. Radding, *J. Mol. Biol.* **18**, 235 (1966); J. W. Little, *J. Biol. Chem.* **242**, 679 (1967).
6. D. M. Carter and C. M. Radding, *J. Biol. Chem.* **246**, 2502 (1971).
7. S. C. Kowalczykowski, D. A. Dixon, A. K. Eggleston, S. D. Lauder, W. M. Rehrauer, *Microbiol. Rev.* **58**, 401 (1994).
8. J. W. Szostak, T. L. Orr-Weaver, R. J. Rothstein, F. W. Stahl, *Cell* **33**, 25 (1983).
9. E. Maryon and D. Carroll, *Mol. Cell. Biol.* **11**, 3278 (1991).
10. M. Lin, K. Sperle, N. Sternberg, *ibid.* **10**, 103 (1990).
11. J. van Oostrum, J. L. White, R. M. Burnett, *Arch. Biochem. Biophys.* **243**, 332 (1985).
12. C. B. Klee and M. F. Singer, *J. Biol. Chem.* **243**, 923 (1968).
13. T. S. Krishna, X. P. Kong, S. Gary, P. M. Burgers, J. Kuriyan, *Cell* **79**, 1233 (1994); X. P. Kong, R. Onrust, M. O'Donnell, J. Kuriyan, *ibid.* **69**, 425 (1992).
14. J. W. Little, I. R. Lehman, A. D. Kaiser, *J. Biol. Chem.* **242**, 672 (1967); S. H. Kim *et al.*, *Science* **185**, 435 (1974); P. M. Colman, J. N. Jansonius, B. W. Matthews, *J. Mol. Biol.* **70**, 701 (1972).
15. L. Holm and C. Sander, *J. Mol. Biol.* **233**, 123 (1993).
16. F. K. Winkler *et al.*, *EMBO J.* **12**, 1781 (1993); D. Kostrewa and F. K. Winkler, *Biochemistry* **34**, 683 (1995).
17. X. Cheng, K. Balendiran, I. Schildkraut, J. E. Anderson, *EMBO J.* **13**, 3927 (1994); A. Athanasiadis *et al.*, *Nature Struct. Biol.* **1**, 469 (1994).
18. U. Selent *et al.*, *Biochemistry* **31**, 4808 (1992).
19. Y. Kim, J. C. Grable, R. Love, P. J. Greene, J. M. Rosenberg, *Science* **249**, 1307 (1990).
20. M. Newman, T. Strzelecka, L. F. Dorner, I. Schildkraut, A. K. Aggarwal, *Nature* **368**, 660 (1994); M. Newman, T. Strzelecka, L. F. Dorner, I. Schildkraut, A. K. Aggarwal, *Science* **269**, 656 (1995).
21. L. S. Beese and T. A. Steitz, *EMBO J.* **10**, 25 (1991).
22. Z. Otwinowski, in *Proceedings of the CCP4 Study Weekend*, L. Sawyer, N. Isaac, S. Borley, Eds. (SERC Daresbury, Daresbury, UK, 1993), pp. 56–62.
23. G. S. French and K. S. Wilson, *Acta Crystallogr.* **A34**, 517 (1978).
24. Collaborative Computational Project, Number 4, *ibid.*, **D50**, 760 (1994).
25. D. E. McRee, *Practical Protein Crystallography* (Academic Press, New York, 1993).
26. Z. Otwinowski, *Daresbury Study Weekend Proceedings* (SERC Daresbury, Daresbury, UK, 1991), pp. 80–89.
27. K. Cowtan, *Joint CCP4 ESF-EACBM Newsletter Protein Crystallogr.* **31**, 34 (1994).
28. T. A. Jones, J. Y. Zou, S. W. Cowan, M. Kjeldgaard, *Acta Crystallogr.* **A47**, 110 (1991).
29. D. E. Tronrud, L. J. Ten Eyck, B. W. Matthews, *ibid.*, **A43**, 489 (1987).
30. R. A. Laskowski, M. W. MacArthur, D. S. Moss, J. M. Thornton, *J. Appl. Crystallogr.* **26**, 283 (1993); A. L. Morris, M. W. MacArthur, E. G. Hutchinson, J. M. Thornton, *Proteins* **12**, 345 (1992).
31. P. J. Kraulis, *J. Appl. Crystallogr.* **24**, 946 (1991).
32. D. J. Bacon and W. F. Anderson, *Mol. Graphics* **6**, 219 (1988); E. A. Merritt and M. E. P. Murphy, *Acta Crystallogr.* **D50**, 869 (1994).
33. A. Nicholls, K. A. Sharp, B. Honig, *Proteins* **11**, 281 (1991).
34. We thank Dr. R. Novy of Novagen for the clone; C. Ogata of the National Synchrotron Light Source, Brookhaven, and B. Miller and M. Szebonyi of CHESS for help with synchrotron data collection; M. Sagermann for advice on crystallographic aspects; D. Tronrud for modifying the TNT refinement package to permit anisotropic scaling; M. Quillin for comments on the manuscript; and R. Myers and members of F. Stahl's group for introducing us to λ-exonuclease. Supported in part by grant GM20066 from the NIH to B.W.M.

15 May 1997; accepted 1 August 1997

25–Hydroxyvitamin D_3 1α-Hydroxylase and Vitamin D Synthesis

Ken-ichi Takeyama, Sachiko Kitanaka, Takashi Sato, Masato Kobori, Junn Yanagisawa, Shigeaki Kato*

Renal 25–hydroxyvitamin D_3 1α-hydroxylase [1α(OH)ase] catalyzes metabolic activation of 25–hydroxyvitamin D_3 into 1α,25–dihydroxyvitamin D_3 [1α,25$(OH)_2D_3$], an active form of vitamin D, and is inhibited by 1α,25$(OH)_2D_3$. 1α(OH)ase, which was cloned from the kidney of mice lacking the vitamin D receptor (VDR$^{-/-}$ mice), is a member of the P450 family of enzymes (P450$_{VD1α}$). Expression of 1α(OH)ase was suppressed by 1α,25$(OH)_2D_3$ in VDR$^{+/+}$ and VDR$^{+/-}$ mice but not in VDR$^{-/-}$ mice. These results indicate that the negative feedback regulation of active vitamin D synthesis is mediated by 1α(OH)ase through liganded VDR.

Vitamin D is metabolized by sequential hydroxylations in the liver and kidney to a family of seco-steroids. The two most biologically active forms of vitamin D are 1α,25$(OH)_2D_3$ and 24R,25–dihydroxyvitamin D_3 [24R,25$(OH)_2D_3$] (*1*, *2*). The binding of 1α,25$(OH)_2D_3$ to the nuclear receptor for the hormonally active form of vitamin D (VDR) activates the VDR (*3*), with subsequent regulation of physiological events such as calcium homeostasis and cellular differentiation and proliferation (*4*). Hydroxylation of 25–hydroxyvitamin D_3 [25$(OH)D_3$] is mediated by 25$(OH)D_3$ 1α-hydroxylase [1α(OH)ase] in the proximal tubule of the kidney. 1α(OH)ase is inhibited by its end product, 1α,25$(OH)_2D_3$ (*5*), and activated by calciotropic peptide hormones such as calcitonin and parathyroid hormone (*6*, *7*). Thus, serum concentrations of 1α,25-$(OH)_2D$ are kept constant. Vitamin D–dependent rickets type I (*8*) may be caused by mutations in the 1α(OH)ase gene. Biochemical analysis of semipurified 1α-(OH)ase protein has suggested that 1α(OH)ase belongs to the P450 family of enzymes (*9*).

We developed a nuclear receptor–mediated expression system to clone the cDNA encoding 1α(OH)ase. This system is based on the fact that a precursor of 1α,25$(OH)_2D_3$, 25$(OH)D_3$, can activate the transactivation function of the VDR only in the presence of 1α(OH)ase activity. Mice lacking the VDR (VDR$^{-/-}$ mice) developed an abnormally high serum concentration of 1α,25$(OH)_2D$ at 7 weeks, suggesting excessive 1α(OH)ase